Available online at www.sciencedirect.com

ScienceDirect

Ceramics International 40 (2014) 4237–4246

CERAMICS INTERNATIONAL

www.elsevier.com/locate/ceramint

Phase equilibria and dielectric properties of $Bi_{3+(5/2)x}Mg_{2-x}Nb_{3-(3/2)x}O_{14-x}$ cubic pyrochlores

P.Y. Tan[a], K.B. Tan[a,*], C.C. Khaw[c], Z. Zainal[a], S.K. Chen[b], M.P. Chon[a]

[a]Department of Chemistry, Faculty of Science, Universiti Putra Malaysia, 43400 UPM Serdang, Selangor, Malaysia
[b]Department of Physics, Faculty of Science, Universiti Putra Malaysia, 43400 UPM Serdang, Selangor, Malaysia
[c]Department of Mechanical and Material Engineering, Faculty of Engineering and Science, Universiti Tunku Abdul Rahman, 53300 Kuala Lumpur, Malaysia

Received 12 June 2013; received in revised form 21 August 2013; accepted 21 August 2013
Available online 29 August 2013

Abstract

Subsolidus pyrochlores with the proposed formula, $Bi_{3+(5/2)x}Mg_{2-x}Nb_{3-(3/2)x}O_{14-x}$ ($0.14 \le x \le 0.22$) were successfully synthesised at the firing temperature of 1025 °C using conventional solid-state reaction. The excess Bi^{3+} charge was offset by removal of relative proportion of Mg^{2+} and Nb^{5+} together with creation of oxygen non-stoichiometry in order to preserve electroneutrality of the system. These samples were crystallised in cubic structure with space group of F*d*3*m*, No. 227 and their refined lattice parameters were in the range of 10.5706 (3)–10.5797 (7) Å. The surface morphologies of the samples as confirmed by scanning electron microscopy analysis were of irregular shaped grains while their crystallite sizes of ~30–85 nm were calculated using the Scherrer equation and the Williamson–Hall method. No thermal event was discernable indicating these pyrochlores were thermally stable within a studied temperature range of ~30–1000 °C. The recorded dielectric constants of $Bi_{3+(5/2)x}Mg_{2-x}Nb_{3-(3/2)x}O_{14-x}$ ($0.14 \le x \le 0.22$) subsolidus pyrochlores were generally above ~160 and their dielectric losses were in the order of 10^{-4}–10^{-3} at the frequency of 1 MHz and temperature of ~30 °C. Meanwhile, these ceramic samples also exhibited negative temperature coefficient of relative permittivity between −528 and −742 ppm/°C in the temperature range of ~30–300 °C.

Keywords: A. Powder: solid-state reaction; C. Impedance; D. Niobates; E. Capacitors; Pyrochlore

1. Introduction

The advent of low temperature co-fired ceramic (LTCC) technology has been impelled by the miniaturisation of modern electronic and electrical devices that require high performance and reliable integrated circuits. Low firing temperature used in LTCC could satisfy the requirements of multichip ceramic modules (MCM), Micro-Electro-Mechanical Systems (MEMS) and Micro-Opto-Electro-Mechanical Systems packages (MOEMS) [1]. By far, dielectric materials in the complex family of bismuth pyrochlores are of great research interest owing to their unique features as they possess high dielectric constant, low dielectric loss and a relative low sintering temperature (< 950 °C) that is compatible with Ag electrode [2–4]. Therefore, bismuth pyrochlores are seriously considered as potential candidates in LTCC towards development of multilayer devices, e.g. capacitors or resonators operating at microwave frequencies.

A comprehensive review of pyrochlores and their structural characteristics have been accounted in literature [5]. The pyrochlore with a general formula, $A_2B_2O_6O'$ could be represented by a complex crystal structure consisting of B_2O_6 octahedral and A_2O' tetrahedral interpenetrating chain networks. Alternatively, it is viewed as a fluorite derivative but with a relatively larger unit cell, $z=8$ [5]. Due to the structural flexibility and variable stoichiometry of pyrochlore family, a wide variety of cation substituents could possibly be introduced in order to enhance their electrical, optical and magnetic properties [5,6]. Among several families of bismuth based pyrochlores, Bi_2O_3–ZnO–Nb_2O_5 (BZN) had been widely investigated and commercialised in ceramic industries since early 70s. Two major phases were reported in which $Bi_3Zn_2Nb_3O_{14}$ (α-BZN) appeared as cubic pyrochlore phase with dielectric constant, ε' of ~150 and had negative temperature coefficient of capacitance, TCC of −500 ppm/°C while monoclinic zirconolite structured, $Bi_2Zn_{2/3}Nb_{4/3}O_{14}$

*Corresponding author. Tel.: +60 389467491; fax: +60 389435380.
E-mail address: tankb@science.upm.edu.my (K.B. Tan).

0272-8842/$ - see front matter © 2013 Elsevier Ltd and Techna Group S.r.l. All rights reserved.
http://dx.doi.org/10.1016/j.ceramint.2013.08.087

(β-BZN) exhibited ε' of ~80 but had positive TCC of +200 ppm/°C [7–9]. The opposite signs of TCC suggested that negative–positive–zero (NPO) devices could be fabricated through careful adjustment of these BZN phases [7].

In attempts to improve the electrical properties of BZN pyrochlores, Mg substituted pyrochlores in Bi_2O_3–MgO–Nb_2O_5 (BMN) ternary had been synthesised and explored for their potential electrical applications. Tremendous studies on BMN system were primarily focused on compositions similar to that of β-BZN analogue, $Bi_2Zn_{2/3}Nb_{4/3}O_7$, a predominantly monoclinic zirconolite phase. However, immediate questions arose as to the existence of $Bi_2Mg_{2/3}Nb_{4/3}O_7$ phase in which its stoichiometry and crystal structure were remained unknown. Nino et al. revealed that $Bi_2Mg_{2/3}Nb_{4/3}O_7$ phase was non-existent as the rigid electronic shell of Mg^{2+} had failed to establish asymmetry Mg–O bond for distorted coordination. On the other hand, α-phase, $Bi_{3/2}MgNb_{3/2}O_7$ in the BMN system was claimed to exist with excess of 15 mole% bismuth that their linear increased lattice parameters obeying Vegard's law [3]. These findings are agreed partially in our unpublished BMN phase diagram results: (i) β-phase is absent but exists as a mixture of α-phase, $Bi_5Nb_3O_{15}$ and a fluorite-like Bi_3NbO_7, (ii) single phase cubic pyrochlores are only formed with compositions that slightly departed from nominal stoichiometry, $Bi_{3/2}MgNb_{3/2}O_7$, i.e. having higher bismuth content. Further explanation is included in Section 3.1.

Despite the uncertainties and inconsistencies on the variable stoichiometry of BMN phases, interesting dielectric properties were reported by several research groups. Cann et al. reported that composition, $Bi_2Mg_{2/3}Nb_{4/3}O_7$ revealed a high ε', 210 with low dielectric loss in the order of 10^{-4} at room temperature and 1 MHz [10]. A similar composition with cation and oxygen vacancies, $(Bi_{2/3\square 1/3})_2(Mg_{1/3}Nb_{2/3})_2O_{6\square 1}$ where □ were vacancies, showed slightly lower ε', 145 and negative TCC in the range of −(342–390) ppm/°C [2]. These results were comparable to that of a related study [11] in which composition, $Bi_{1.67}Mg_{0.75}Nb_{1.5}O_7$ exhibited ε' of 151 and tan δ of 0.0004 at 100 kHz. Although varying values had been found but the authors may have agreed that dielectric properties of BMN phases had strong reliance on the compositions and structures.

On the other hand, investigations on electrical properties were also performed using BMN thin films deposited by different deposition techniques, e.g. pulse laser deposition (PLD), RF magnetron sputtering and spin-coating methods on various substrates and electrodes [4,12–17]. $Bi_{1.5}MgNb_{1.5}O_7$ thin films annealed at 750 °C on Au-coated Si substrates by RF magnetron sputtering exhibited moderate dielectric constant of ~106 and low dielectric loss of 0.003–0.007 between 10 kHz and 10 MHz [12]. Similar result was reported for $Bi_{1.5}MgNb_{1.5}O_7$ thin film annealed at 700 °C on platinum-coated sapphire that had tunability up to 50% at a bias field of 1.5–2 MV/cm [12–14]. In the case of β-phase, $Bi_2Mg_{2/3}Nb_{4/3}O_7$ thin films deposited by PLD on $Ti/SiO_2/Si$ substrates with Pt or Cu electrode revealed a significant drop in their dielectric constants with values, 51 and 56, respectively [4]. A related study was performed by Park et al. in an embedded $Bi_2Mg_{2/3}Nb_{4/3}O_7$ thin film capacitor; 130-nm-thick film deposited on polymer (copper clad laminate) substrate at 150 °C exhibited a dielectric constant of 47, capacitance density of approximately 302 nF/cm^2 and breakdown strength of 0.7 MV/cm [16]. Whilst, high dielectric constant associated with ferroelectric relaxor behaviour was also claimed in spin coated $Bi_2Mg_{2/3}Nb_{4/3}O_7$ thin film on Si(100) substrate [15]. Regardless of the deposition techniques used, dielectric response of the prepared thin films was postulated to be essentially influenced by the quality of the film. Careful attention was therefore required to control annealing condition, surface roughness, thickness, interfacial layer and also the selection of substrate and electrode [4,12–17].

In this paper, we report on the phase formation of 'bismuth-rich' BMN α-phases with the proposed formula of $Bi_{3+(5/2)x}Mg_{2-x}Nb_{3-(3/2)x}O_{14-x}$ $(0.14 \le x \le 0.22)$. The subsolidus solution limit is found slightly narrower if compared to that of our reported cubic pyrochlores in the Bi_2O_3–MgO–Ta_2O_5 (BMT) analogous system [18]. For better understanding of these BMN α-phases, the results concerning their structural and electrical properties at different temperatures and frequencies are investigated and presented herewith.

2. Experimental

The conventional solid-state method was applied in sample synthesis of which compositions with the proposed formula, $Bi_{3+(5/2)x}Mg_{2-x}Nb_{3-(3/2)x}O_{14-x}$ (x=0, 0.12–0.24) were prepared. Reagent grade oxide powders, Bi_2O_3 (Alfa Aesar, 99.99%), MgO (Aldrich, 99%) and Nb_2O_5 (Alfa Aesar, 99.9%) were used as starting materials that dried at 300 °C for Bi_2O_3 and 600 °C for MgO and Nb_2O_5, respectively. Stoichiometric amount of oxides were weighed and then ground in sufficient acetone using an agate mortar and pestle. The mixed powders were then carefully transferred into platinum boats for calcinations. The samples were pretreated at 300 °C for 1 h and further heated at 600 °C for 1 h to ensure the Bi_2O_3 reacted to form less-volatile compounds; this allowed firing at higher temperatures without significant losses of bismuth. The pretreated powders were heated at 800 °C overnight and further synthesised at 1025 °C for 2–3 days with intermediate regrinding to ensure their thermal equilibrium. The powders were pressed into pellets (8 mm in diameter and ~1.5 mm in thickness) and sintered at 1050 °C for 24 h to achieve relative densities of higher than 90%. X-ray powder diffraction technique was used to examine the phase purity of the samples using an automated Shimadzu diffractometer XRD 6000, Cu Kα radiation in 2θ range of 10–70° at the scan speed of 2 deg/min. Data collected at the scan rate of 0.1 deg/min were used for lattice parameter refinement by Chekcell software [19]. The surface microstructures of the as fired pellets were investigated by scanning electron microscope (SEM, JOEL JSM-6400). Infrared analysis was carried out in the range of 280–4000 cm^{-1} using an ATR (Attenuated total reflectance) coupled Perkin Elmer Fourier transform infrared spectrometer. Thermal analyses of the phase pure samples were studied by thermogravimetry (TG) and differential thermal

analysis (DTA). Both Perkin Elmer instruments, TGA 7 and DTA 7 were used for heat cycle in temperature range of ~30–1000 °C with a heating rate of 10 °C/min whereas the cool cycle was only performed in DTA analysis with a cooling rate of 10 °C/min. The electrical properties measurements were carried out using AC impedance analyser, Hewlett-Packard, HP4192A in the frequency range from 5 Hz to 13 MHz at various temperatures (~30–850 °C). Pellets were optimised as reported in [9] prior to correction for their geometrical factors and stray capacitance of an open jig. The pellet with gold electrodes was then attached firmly to conductivity jig and electrical measurement was performed in temperature controlled horizontal tube furnace for every 50 °C interval at an equilibrium time of ~25 min upon a heat-cool cycle.

3. Results and discussion

3.1. XRD analysis

The prepared subsolidus $Bi_{3+(5/2)x}Mg_{2-x}Nb_{3-(3/2)x}O_{14-x}$ ($0.14 \le x \le 0.22$) pyrochlores are fully indexed with space group, F*d*3*m*, No. 227 as shown in their XRD patterns (Fig. 1a). Phase pure samples are confirmed by the absence of characteristic diffraction peaks of secondary phases. Introduction of higher Bi content in BMN pyrochlores is proposed to be compensated by a decrease in Mg and Nb together with a variation of oxygen content. The subsolidus solution mechanism could be summarised as below in which the overall charge neutrality is prevailed.

$$5/2Bi^{3+} \leftrightarrow Mg^{2+} + 3/2Nb^{5+} + O^{2-} \quad (1)$$

Interestingly, the reported nominal composition, $Bi_3Mg_2Nb_3O_{14}$, i.e. $x=0$ is excluded from BMN subsolidus solution and single phase cubic pyrochlores are only formed with minimum Bi mole% of ~41.75%. At lower limit, compositions with $x < 0.14$ contain secondary phases of $MgNb_2O_6$ and $Mg_4Nb_2O_9$ that coexisted with cubic pyrochlore in an associated three-phase assemblage. Meanwhile, compositions with $x > 0.22$ are a mixed phase containing traceable amount of $Bi_5Nb_3O_{15}$ and Bi_3NbO_7 phases. The minute peaks (Fig. 1b) at 2 theta values, 28.62 ° and 34.36 ° are ascribed to $Bi_5Nb_3O_{15}$ (ICDD no. 39-939) while 32.782 ° is identified as Bi_3NbO_7 (ICDD no. 50-87). It is worthwhile to highlight that neither $Bi_3Mg_2Nb_3O_{14}$ nor $Bi_2Mg_{2/3}Nb_{4/3}O_7$ is single phase as they fall into two different compatible phase assemblages consisting of pyrochlore–$MgNb_2O_6$–$Mg_4Nb_2O_9$ and pyrochlore–$Bi_5Nb_3O_{15}$–Bi_3NbO_7, respectively. This result is somewhat contradictory to that reported in [3], in which excess bismuth of 15 mole% is permissible in BMN subsolidus pyrochlores.

In order to explain the subsolidus formation, it is useful to invoke detailed pyrochlore structure, $A_2B_2O_6O'$ of which there are two distinct cation crystallographic sites. Typically, A-site is predominantly occupied by the larger cations that are in eight-fold coordination while the smaller B site cations will have a reduced six-fold coordination. The larger Bi cation preferentially occupies eight-coordinated A site whereas B site cation, Nb usually adopts octahedral coordination with O(1). It

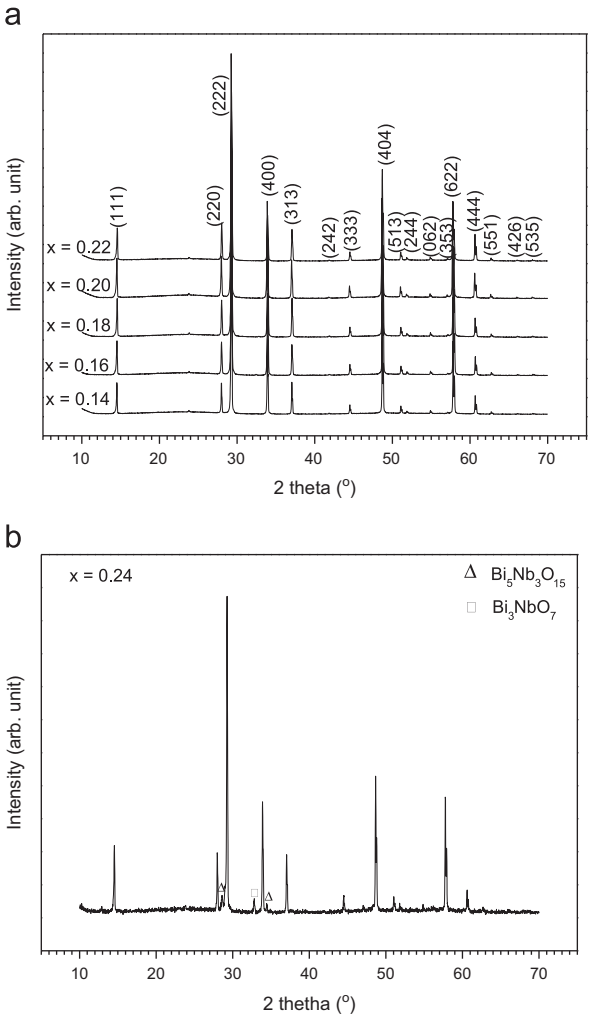

Fig. 1. (a) XRD patterns of $Bi_{3+(5/2)x}Mg_{2-x}Nb_{3-(3/2)x}O_{14-x}$ ($0.14 \le x \le 0.22$) solid solution (b) XRD pattern of $Bi_{3+(5/2)x}Mg_{2-x}Nb_{3-(3/2)x}O_{14-x}$, $x=0.24$.

is interesting enough that Mg cation is able to occupy both A and B sites as similar to that of our reported Ta analogue [18]. Assuming full occupancy on both A and B sites, the cation ratios on the A-site and B-site are set to $(Bi_{3.35}Mg_{0.65})(Mg_{1.21}Nb_{2.79})O_{13.86}$ for $x=0.14$, in which the Bi:Mg is 0.8375:0.1625 and Mg:Nb is 0.3025:0.6975, respectively. As x value increases, higher Bi content is desirable and such increment will be compensated by lower Mg content at A site yielding higher Bi:Mg cation ratio [3,18,20]. Such predilection could be explained from the chemical point of view as Mg cation is considered too small to fit into an eight-coordinated A site; therefore, higher bismuth concentration in A site is somewhat expected to stabilise and/or to reduce the disordered pyrochlore structure. However, full Bi occupancy on A site should be avoided as this may lead on to pyrochlore cell distortion arising from the coupling effect of Bi $6s^2$ lone pair electrons [21]. In addition to this, Mg^{2+} will reside more comfortably in B site due to its larger ionic radius, 0.72 Å if compared to that of Nb^{5+}, 0.64 Å under a six-fold coordination [22]. Consider the qualitative analyses on compositional variables and available structural information, BMN cubic

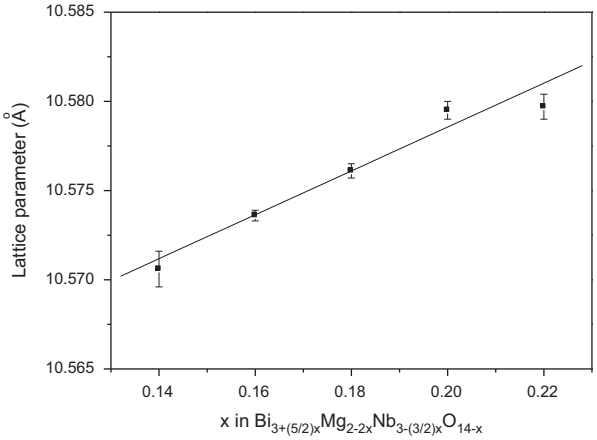

Fig. 2. Variation of lattice parameters in $Bi_{3+(5/2)x}Mg_{2-x}Nb_{3-(3/2)x}O_{14-x}$ $(0.14 \le x \le 0.22)$ pyrochlores.

pyrochlores are anticipated to be less disordered in particularly this is attributed to the effect of self-compensation of cation occupancy and redistribution of cations over both A and B sites. It is also believed that the displacement of smaller cation at A site like the reported α-BZN analogue towards higher multiplicity site, i.e. 96 g to achieve lower coordination environment could be reduced [20,23,24]. On the other hand, lattice parameters of the prepared compositions are found to increase gradually from 10.5706 (3) to 10.5797 (7) Å (Fig. 2). There is an almost linear positive relation between lattice parameters with compositions x for which Vegard's law is obeyed [18]. Increase of Bi content has resulted in unit cell expansion due to the larger Bi ionic radius, Bi^{3+} (1.17 Å) if compared to that of Mg^{2+} (0.89 Å) under an eight-fold coordinated A site [3,22]. However, all postulations made herewith will certainly require further confirmation from detailed structural refinement combining sophisticated X-ray, neutron diffraction and electron microscopy studies.

3.2. Grain size and microstructure

The surface morphologies of the as-fired pellets are shown in the SEM micrographs (Fig. 3). The grain sizes of the samples are in the range of 1.75–13.00 μm with irregular shape after sintering at temperature of 1050 °C for 1 day. The relative densities are in general higher than 90% of the theoretical value, showing good and dense pellets. Polycrystalline BMN pyrochlores are in general composed of crystal aggregates or grains derived from approximately hundred of crystallites. Determination of the mean crystallite size, C_{size} of the samples is calculated based on the Scherrer equation.

$$C_{size} = (k \times \lambda)/(\beta \times \cos\theta) \quad (2)$$

where k is a constant, 0.90, λ is the wavelength, β is the full width at half maximum (FWHM) of the peak, and θ is the angular position of the peak. The calculated crystallite sizes of the samples with the Scherrer equation are in the range of 53–82 nm (Fig. 4). On the other hand, the Williamson–Hall (W–H) method is also used to examine the line broadening that may have attributed to simultaneous small crystallite size and lattice strain [25]. The correlation between internal strain and crystallite size is portrayed as below:

$$(\beta \cos\theta)/\lambda = 0.9/d_{avg} + (4\varepsilon \sin\theta)/\lambda \quad (3)$$

where 0.9 is the shape factor, λ is the CuK_α radiation of wavelength ($\lambda = 1.5418$ Å), β is the FWHM, ε is the strain, and θ is the scattering angle. The crystallite sizes obtained by the W–H method are in the range of 33–69 nm (Fig. 4) and this result is comparable to those calculated through the Scherrer method. The calculated strain, ε values for all prepared compositions are in the order of 10^{-4} implying that the structural deformation in BMN pyrochlores is negligibly small (Fig. 5). This finding also supports the absence of cell distortion that associated with the shape of (111) and (222) XRD peaks in BMN pyrochlores [3]. Summary of the calculated internal strain, crystallite sizes from two different methods and grain sizes (SEM) is shown in Table 1.

3.3. IR and thermal analysis

Infrared-active phonon modes have been assigned to specific bending and stretching vibrational modes that originated from vibration and bending of metal-oxygen bond in BMN pyrochlores (Fig. 6). The B–O stretching vibration is observed in the region of 570–630 cm^{-1} and the broad characteristic may due to the overlapping vibrations of Nb–O and Mg–O. The splitting modes of B–O stretching, ω_1 and ω_1^* are in principle due to force-constant or mass effects and the lighter ions will tend to vibrate at higher frequency. Hence, the phonon modes, ω_1 (622–631 cm^{-1}) and ω_1^* (570–577 cm^{-1}) are assigned to Mg–O stretching and Nb–O stretching, respectively [26].

The phonon mode, ω_2 at wavenumber ~470–490 cm^{-1} is corresponded to the vibration of the longer A–O′ bond, while phonon mode, ω_n^{**} (~840–850 cm^{-1}) is due to the shorter A–O′ bond. The disordered phonon mode between A and O′ ions may have resulted from static displacement in pyrochlore structure especially a much smaller cation, e.g. Mg shares eight-coordinated A site with larger Bi [18,26]. The phonon mode, ω_3 is assigned to A–O stretching in the region ~300–340 cm^{-1} and this is probably attributed to Bi–O bond. The observed infrared phonon modes of BMN pyrochlores are summarised in Table 2.

Figs. 7 and 8 show thermograms of BMN samples in the studied temperature ranging from ~30 °C to 1000 °C. DTA and TGA are complementary techniques that used to confirm thermal stability of BMN pyrochlores. No thermal event is discernable as the prepared BMN pyrochlores are impervious to any thermal changes once their thermal equilibrium state has been reached. The reported polymorphic transition of a monoclinic structured, β-BZN phase into cubic symmetry is again not observed in the case of BMN pyrochlore [3].

3.4. Electrical properties

Impedance spectroscopy is a versatile technique to probe the electrical behaviours of materials under the influence of different applied voltages, frequencies and temperatures [27].

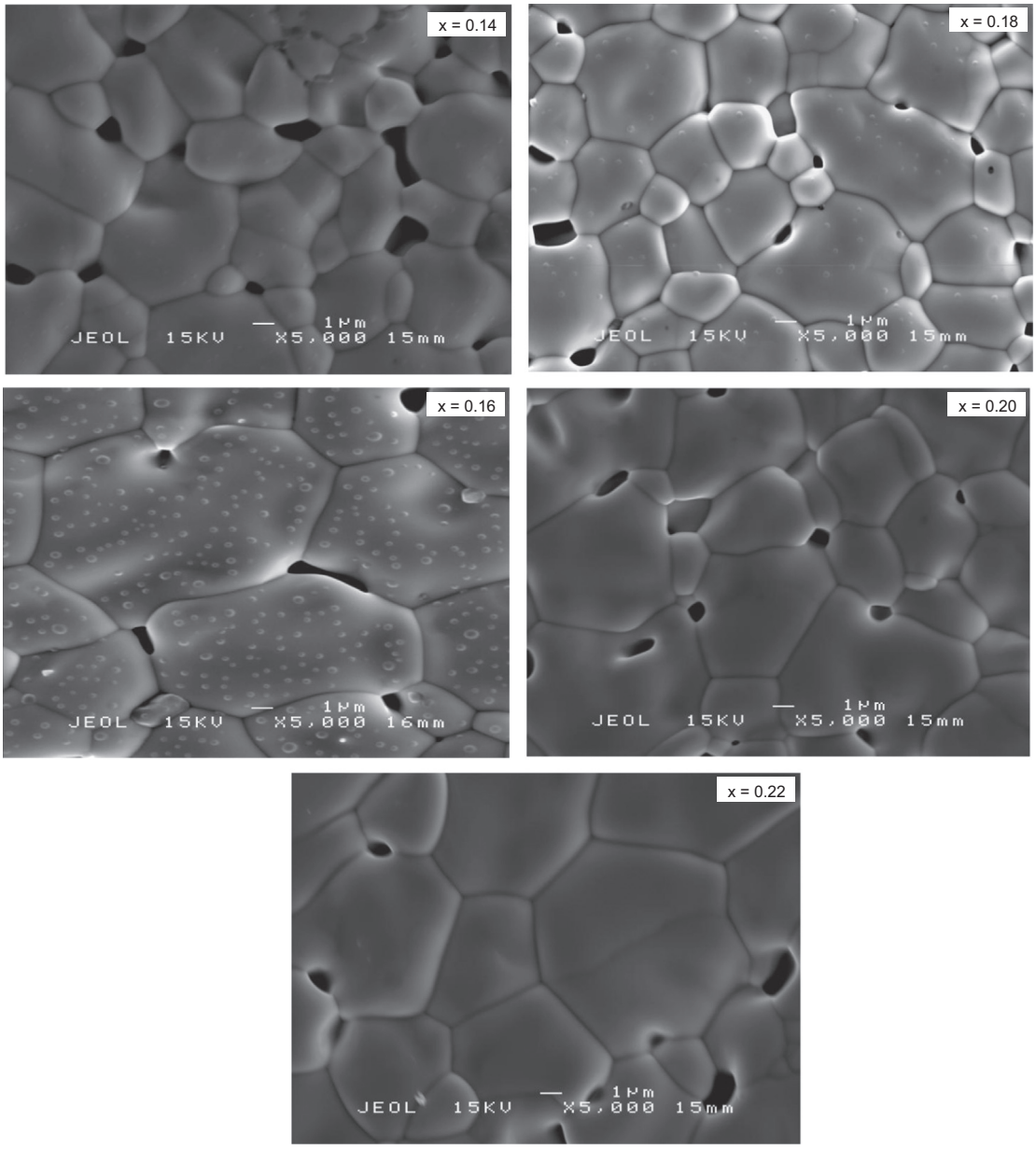

Fig. 3. SEM micrographs of $Bi_{3+(5/2)x}Mg_{2-x}Nb_{3-(3/2)x}O_{14-x}$ ($0.14 \le x \le 0.22$) recorded at magnification of 5 k.

The electrical response could be represented by careful circuit fitting method based on different equivalent circuits consisting of a pair and/or more RC elements that connected in parallel or series. Prior to measurement, all collected impedance data are normalised by samples' geometric factors and corrected for stray capacitance of open jig. All BMN cubic pyrochlores exhibit similar characteristics on various electrical characterisation plots and therefore, only composition, $Bi_{3.50}Mg_{1.80}Nb_{2.70}O_{13.80}$ ($x=0.20$) is illustrated for further explanation. A perfect semicircle can be seen in the complex impedance plot, Z'' versus Z' of $Bi_{3.50}Mg_{1.80}Nb_{2.70}O_{13.80}$ ($x=0.20$) at 598 °C (Fig. 9). Equivalent circuit can be modelled from the electrical response of this sample and the impedance data is well fitted by a single RC element that arranged in parallel, with both bulk resistance, R_b and bulk capacitance, C_b [18,27]. The associated capacitance value of $Bi_{3.50}Mg_{1.80}Nb_{2.70}O_{13.80}$ at $\omega RC=1$ is 11.2 pF cm^{-1} at 598 °C, 1 MHz showing typical bulk response [18].

According to detailed impedance formalisms, Debye response peaks could be evidently shown in a spectroscopic plot combining imaginary components Z'' and M'' against logarithmic frequency function. The Debye peak maxima, for each RC element is correlated with time constant as shown in below.

$$\omega_{max} = 2\pi f_{max} = (RC)^{-1} = \tau^{-1} \quad (4)$$

where ω, τ, and f correspond to angular frequency, time constant and frequency, respectively. Meanwhile, the magnitudes of R and C could be calculated from Z''_{max} and M''_{max} as demonstrated by equations below [27,28].

$$Z''_{max} = R/2 \quad (5)$$

$$M''_{max} = \varepsilon_o/(2C) \quad (6)$$

where ε_o is the permittivity of free space (8.854×10^{-14} F cm^{-1}).

The peaks of M'' and Z'' are coincident at high frequency region showing an almost perfect Debye of 1.15 decades (Fig. 10). Ideally, the full width at half maximum (FWHM) of the M'' peak should be 1.14 decades for an electrically homogeneous material. The close agreement between these two values indicates that the electrical response of $Bi_{3.50}Mg_{1.80}Nb_{2.70}O_{13.80}$ is primarily due to the bulk response but not other components such as grain boundary. Furthermore, no grain boundary or blocking electrode effect is seen at low frequency region of the complex impedance plot (Fig. 9) and this provides additional evidence that this material is electrically homogeneous [18,27,29]. For heterogeneous materials, more than one RC elements are postulated in which the spectroscopic M'' spectrum may show additional and/or broaden peak [27]. Different capacitance values calculated

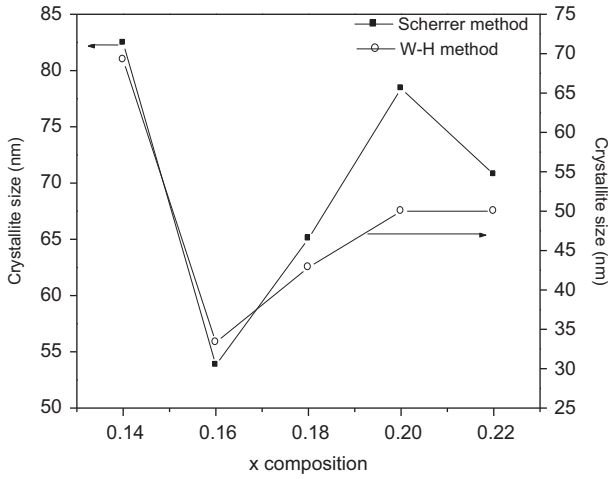

Fig. 4. Comparison of crystallite sizes between Scherrer and Williamson–Hall methods for $Bi_{3+(5/2)x}Mg_{2-x}Nb_{3-(3/2)x}O_{14-x}$ ($0.14 \le x \le 0.22$) pyrochlores.

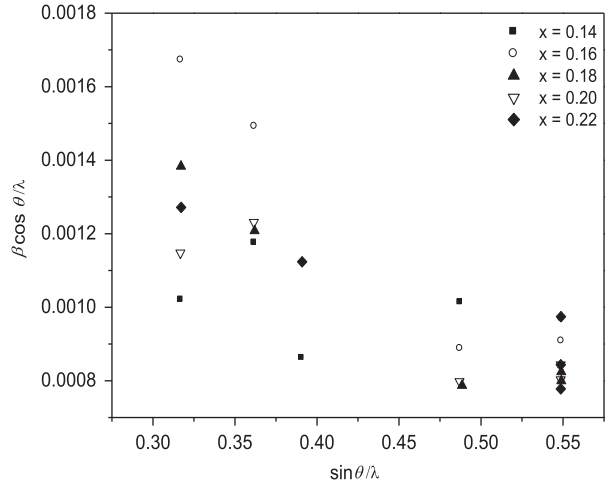

Fig. 5. Williamson–Hall plots of $Bi_{3+(5/2)x}Mg_{2-x}Nb_{3-(3/2)x}O_{14-x}$ ($0.14 \le x \le 0.22$) pyrochlores.

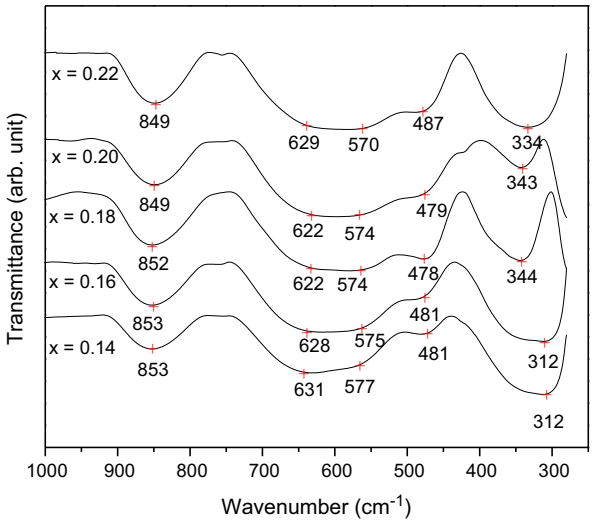

Fig. 6. IR spectra of $Bi_{3+(5/2)x}Mg_{2-x}Nb_{3-(3/2)x}O_{14-x}$ ($0.14 \le x \le 0.22$) solid solution.

Table 2
Infrared spectra and observed phonon modes of BMN pyrochlores.

x						
Mode	Mode assignment	Wavenumber (cm^{-1})				
		0.14	0.16	0.18	0.20	0.22
ω_n^{**}	(A–O′) stretch	853	853	852	849	849
ω_1	(B–O) stretch	631	628	622	622	629
ω_1^{*}	(B–O) stretch*	577	575	574	574	570
ω_2	(A–O′) stretch	481	481	478	479	487
ω_3	(A–O) stretch	312	312	344	343	334

Table 1
Calculated grain sizes, crystallite sizes and strains of $Bi_{3+(5/2)x}Mg_{2-x}Nb_{3-(3/2)x}O_{14-x}$, ($0.14 \le x \le 0.22$) pyrochlores.

x	C_{size}=average crystallite size		W–H plot, strain (ε)	Grain size, (μm)
	Scherrer (nm)	W–H method (nm)		
0.14	82	69	0.00020	1.75–6.75
0.16	53	33	0.00083	2.50–13.00
0.18	65	42	0.00063	1.75–8.75
0.20	78	50	0.00045	2.25–8.75
0.22	70	50	0.00043	3.00–9.50

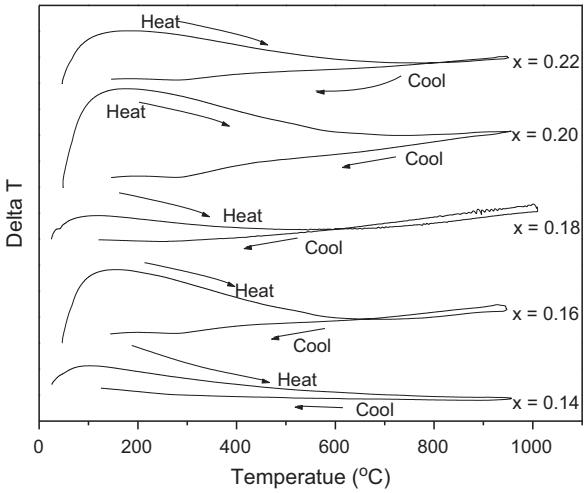

Fig. 7. DTA thermograms of $Bi_{3+(5/2)x}Mg_{2-x}Nb_{3-(3/2)x}O_{14-x}$ ($0.14 \le x \le 0.22$) solid solution.

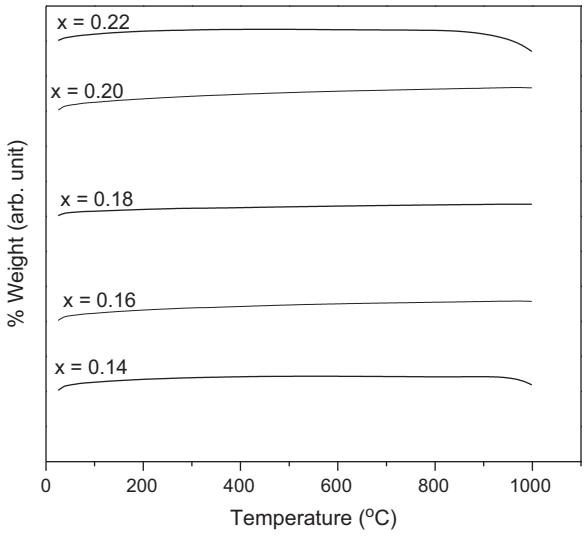

Fig. 8. TGA thermograms of $Bi_{3+(5/2)x}Mg_{2-x}Nb_{3-(3/2)x}O_{14-x}$ ($0.14 \le x \le 0.22$) solid solution.

from Eqs. (4) and (6) could then use to assign the electrical responses, e.g. materials contained grain boundary or secondary phase would have capacitance value in the order of 10^{-11} F cm^{-1} [27].

The imaginary part of complex impedance, Z'' is plotted against frequency on logarithmic scales at various temperatures (Fig. 11). The displacement of peak maxima with increasing frequency at higher temperatures indicates a decrease of R values (Eq. 5) as a low-conductivity pathway is probably feasible due to the thermal destruction of local structure. This phenomenon could also be associated with thermally induced charge carrier polarisation that is found in typical dielectric materials [29]. Different types of polarisation are generally proposed for materials with high dielectric constant and this includes mechanisms involving electronic polarisation, ionic or atomic polarisation, dipole polarisation and space charge polarisation [30]. The occurrence of these processes may

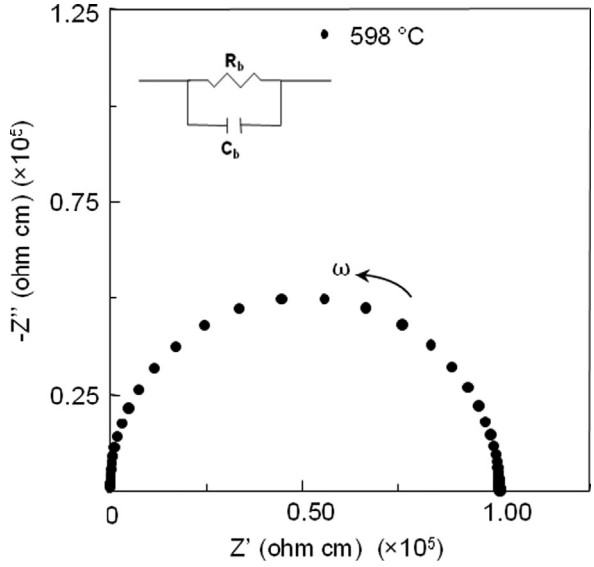

Fig. 9. Complex impedance plot of $Bi_{3.50}Mg_{1.80}Nb_{2.70}O_{13.80}$ at 598 °C.

interestingly overlap one another or takes place independently. In the case of bismuth-based pyrochlores, it had been proposed that dielectric relaxation could be of glass-like relaxor behaviour that involved compositional or structural heterogeneity [3,31]. The smaller Mg at eight coordinated A site in BMN cubic pyrochlores could have caused disruption of local translational symmetry and the resulted disordered structure may account for the dielectric polarisation process [3]. On the other hand, the origin of high polarisation found in Mg-deficient BMN pyrochlore had been inferred to the structured diffusion of A site cation, e.g. Bi^{3+} or Mg^{2+}. This was further supported by the local structure study using electron diffraction and bond valence sum (BVS) analyses of which the displacive shift in $O'A_2$ sub-structure was responsible for strain induced structural relaxation and creation of local dipole moments [11]. At this stage, there is yet any conclusive explanation for high dielectric constant found in BMN pyrochlores, but the possible mechanisms of polarisation are at least fairly understood now.

The conductivity values of BMN pyrochlores at different temperatures are deduced from the high intercept of real impedance in typical complex Cole–Cole plots (Fig. 9). These values are then tabulated in accordance with the Arrhenius conductivity equation

$$\sigma = \sigma_o \exp(-E_a/k_B T) \quad (7)$$

where σ_o is the conductivity at infinite temperature, whilst T, k_B and E_a are, respectively absolute temperature, Boltzmann's constant and activation energy for conduction. The thermally activated electrical conduction of BMN pyrochlores requires activation energies (slopes of Fig. 12) in the range of 1.20–1.37 eV. High activation energy, e.g. >1.0 eV could be associated with a hopping type of electronic transport mechanism if not linked to the ionic conduction and this agrees reasonably with those mentioned earlier [18,29]. On the other hand, activation energy in relaxor materials had been claimed to increase with higher volume of the coherent polarising unit [3,32]. For BMN cubic pyrochlores, higher coherent polarisation volume is expected

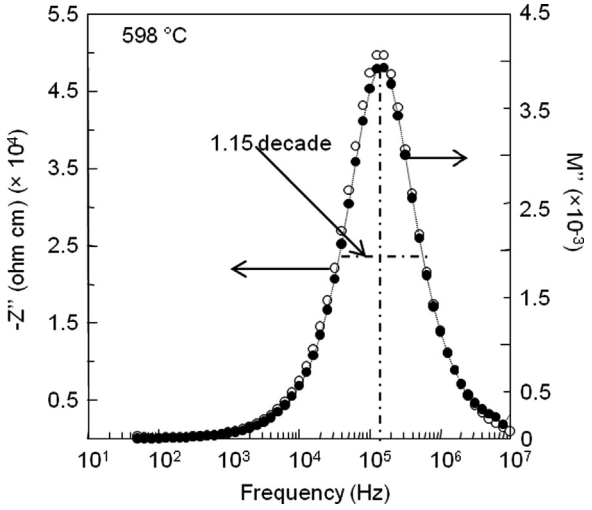

Fig. 10. Combine spectroscopic plots of $Bi_{3.50}Mg_{1.80}Nb_{2.70}O_{13.80}$.

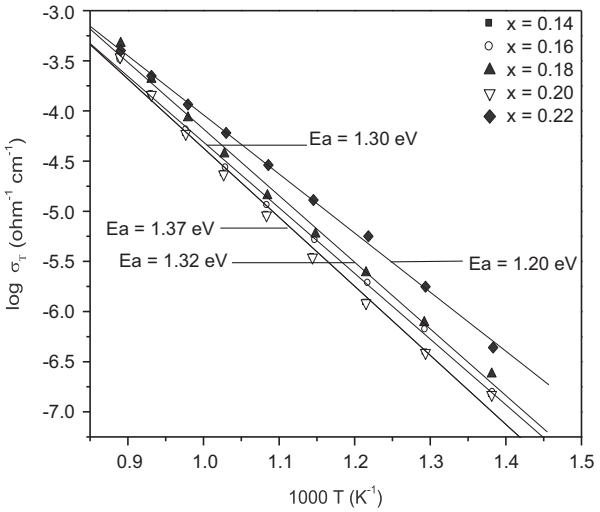

Fig. 12. Arrhenius conductivity plots of $Bi_{3+(5/2)x}Mg_{2-x}Nb_{3-(3/2)x}O_{14-x}$ $(0.14 \le x \le 0.22)$ pyrochlores.

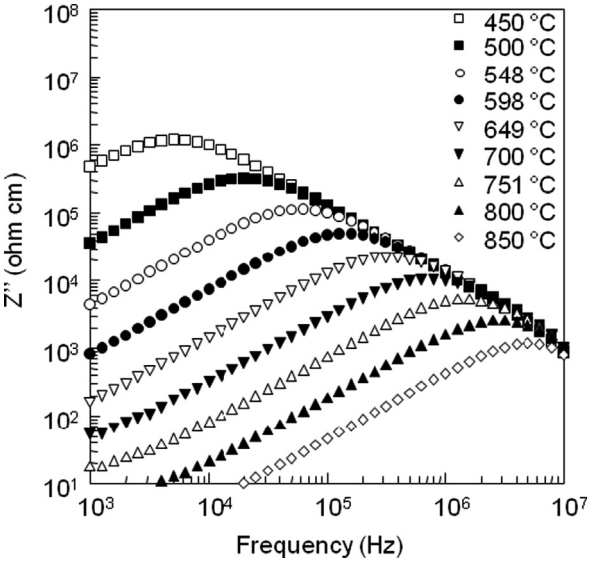

Fig. 11. Imaginary part of impedance plotted as a function of frequency at different temperatures for composition, $Bi_{3.50}Mg_{1.80}Nb_{2.70}O_{13.80}$.

from fewer local symmetry breaks that may have resulted from reduction of Mg at A site [3]. However, no systematic shift is observed as this could be probably attributed to a small variation of Mg occupancy at A site, i.e. lower than 5%. The electrical properties of the BMN pyrochlores are summarised in Table 3.

Dielectric materials fulfil circuit functions of which their dielectric constant, ε', and dielectric loss, $\tan\delta$, are of indicatives for their relative ability of stored capacitance and energy loss, respectively. These parameters are correlated in equations as shown below.

$$\varepsilon^*(\omega) = \varepsilon'(\omega) - \varepsilon''(\omega) \tag{8}$$

$$\tan\delta = \varepsilon''/\varepsilon' \tag{9}$$

BMN pyrochlores exhibit good bulk dielectric properties with ε' values in the range of 167–204 and low dielectric losses, in the order of 10^{-4}–10^{-3} at ambient temperature and frequency of 1 MHz (Fig. 13). As x increases, higher ε' values are recorded for BMN pyrochlores with higher Bi content and this is probably due to the increase of polarisation volume which mentioned earlier. Meanwhile, higher polarisation could also be attributed to the fact that Bi^{3+} has higher polarisability, $\alpha = 6.12$ Å^3 than that of Mg^{2+}, $\alpha = 1.32$ Å^3 [18,33]. It is also clear that ε' values of the prepared BMN pyrochlores are generally higher than the reported $Bi_2Mg_{2/3}Nb_{4/3}O_7$ thin films and other bismuth-rich compositions [3,4,16,17] but are comparable to that of reported $Bi_{1.5}MgNb_{1.5}O_7$ thin film, e.g. ε' values in a range of ~165–195 [13,14]. As compared to BMT analogues, BMN pyrochlores exhibit superior performance as the measured ε' values are almost three-fold higher [18]. The key B ion in the centre of BO_6 octahedra, e.g. Nb_2O_5 could be responsible for this as it has an average higher dielectric constant than that of Ta_2O_5 in various symmetry forms [8,34–36].

The temperature coefficient of relative permittivity, TCε' is calculated in a temperature range of ~30–300 °C and BMN pyrochlores generally have negative TCε' in the range of −528 ppm/°C to −742 ppm/°C (Fig. 14). These values are comparable to that of reported values, −750 ppm/°C to +110 ppm/°C in various pyrochlore types [2]. Interestingly, ε' of BMN pyrochlores is also found to decrease with increasing temperatures. Such phenomenon could have resulted from the thermal disruption of dipoles in BMN pyrochlores. The variation of $\tan\delta$ as a function of temperature for different BMN compositions at fixed frequency of 1 MHz is illustrated in Fig. 15. At low temperatures, $\tan\delta$ of the BMN pyrochlores are non-temperature dependent, a common behaviour for low-loss materials with 'flat' spectra response [30]; but an appreciable increase is observed at temperatures above 600 °C. At high temperatures, influx of thermally activated charge carrier could cause increase of real admittance and this contributes towards higher dielectric loss in conduction mechanism [18,29,35].

Table 3
Summary of electrical properties of cubic pyrochlores in bismuth magnesium niobate ternary system.

x	Dielectric constant, ε'	Dielectric loss, tan δ	Temperature coefficient of relative permittivity, TCε'	Activation energy, E_a (eV)
0.14	167	0.0008	−528	1.37
0.16	188	0.0013	−711	1.30
0.18	187	0.0008	−591	1.32
0.20	195	0.0041	−742	1.37
0.22	204	0.0005	−685	1.20

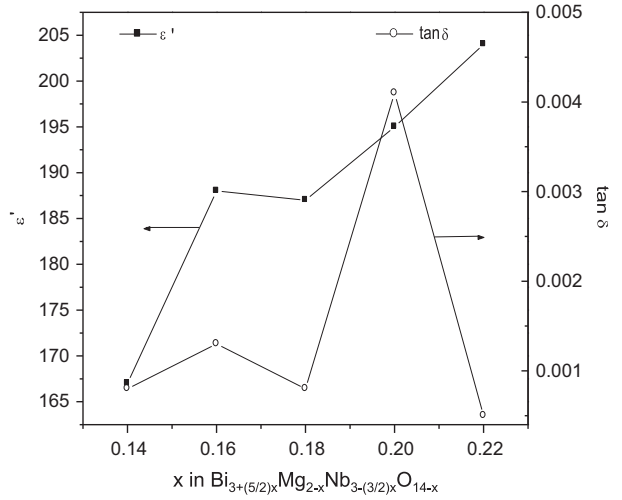

Fig. 13. Dielectric constants and dielectric losses of BMN cubic pyrochlores at 30 °C at 1 MHz.

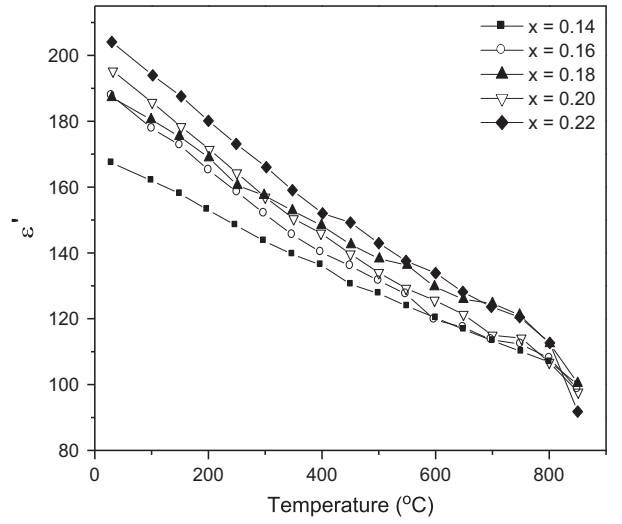

Fig.14. Temperature dependence of dielectric constants of BMN cubic pyrochlores at fixed frequency 1 MHz.

4. Conclusion

Subsolidus $Bi_{3+(5/2)x}Mg_{2-x}Nb_{3-(3/2)x}O_{14-x}$ pyrochlores in bismuth magnesium niobate ternary system had been successfully synthesised and the solid solution limit was confirmed as $0.14 \leq x \leq 0.22$. Increase of Bi content did not cause any significant structural deformation in BMN cubic pyrochlores

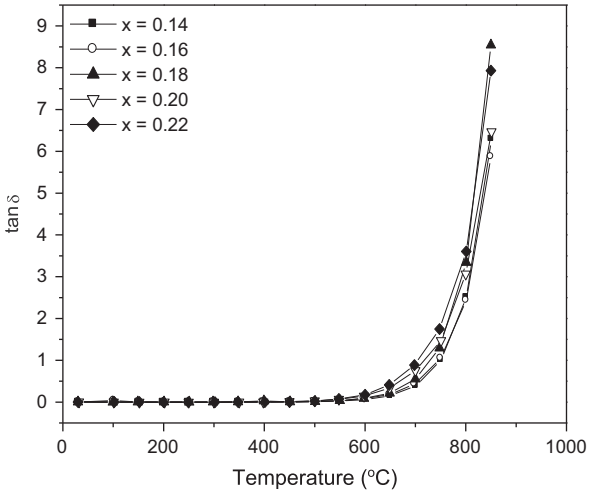

Fig. 15. Temperature dependence of dielectric losses BMN cubic pyrochlores at fixed frequency of 1 MHz.

but allowed further enhancement on their dielectric properties. These materials revealed high dielectric constants with the values in the range of 167–204 and low dielectric losses in the order of 10^{-4}–10^{-3} at room temperature and frequency of 1 MHz. BMN pyrochlores possessed high activation energies in the range of 1.20–1.37 eV suggesting that the conduction mechanism could be of electronic hopping-type.

Acknowledgements

We are grateful for financial support from Ministry of Higher Education, Malaysia via Research University Grant Scheme (RUGS) and P.Y. Tan thanks for her National Science Fellowship (NSF) from the Ministry of Science, Technology, and Innovation Malaysia (MOSTI).

References

[1] L.J. Golonka, Technology and applications of Low Temperature Cofired Ceramic (LTCC) based sensors and Microsystems, Bulletin of the Polish Acacdemy of Sciences: Technical Sciences 54 (2006) 221–231.
[2] E.A. Nenasheva, N.F. Kartenko, Low-sintering ceramic materials based on Bi_2O_3–ZnO–Nb_2O_5 compounds, Journal of the European Ceramic Society 26 (2006) 1929–1932.
[3] J.C. Nino, H.J. Youn, M.T. Lanagan, C.A. Randall, Bi_2O_3 solubility of Bi-based pyrochlores and related phases, Journal of Materials Research 17 (2002) 1178–1182.
[4] C.J. Xian, J.H. Park, K.C. Ahn, S.G. Yoon, J.W. Lee, W.C. Kim, S.T. Lim, S.H. Sohn, J.S. Moon, J.M. Jung, S.E. Lee, I.H. Lee,

Y.K. Chung, M.K. Jeon, S.I. Woo, Electrical properties of $Bi_2Mg_{2/3}Nb_{4/3}O_7$ (BMN) pyrochlore thin films deposited on Pt and Cu metal at low temperatures for embedded capacitor applications, Applied Physics Letters 90 (2007) 052903.

[5] M.A. Subramanian, G. Aravamudan, G.V. Subba Rao, Oxide pyrochlores—a review, Progress in Solid State Chemistry 15 (1983) 55–143.

[6] H.J. Youn, C. Randall, A. Chen, T. Shrout, M.T. Lanagan, Dielectric relaxation and microwave dielectric properties of Bi_2O_3–ZnO–Ta_2O_5 ceramics, Journal of Materials Research 17 (2002) 1502–1506.

[7] H. Wang, H. Du, Z. Peng, M. Zhang, X. Yao, Improvements of sintering and dielectric properties on Bi_2O_3–ZnO–Nb_2O_5 pyrochlore ceramics by V_2O_5 substitution, Ceramics International 30 (2004) 1225–1229.

[8] H. Du, X. Yao, Synthesis and dielectric properties development of new thermal stable bismuth pyrochlores, Journal of Physics and Chemistry of Solids 63 (2002) 2123–2128.

[9] C.C. Khaw, K.B. Tan, C.K. Lee, A.R. West, Phase equilibria and electrical properties of pyrochlore and zirconolite phases in the Bi_2O_3–ZnO–Ta_2O_5 system, Journal of the European Ceramic Society 32 (2012) 671–680.

[10] D.P. Cann, C.A. Randall, T.R. Shrout, Investigation of the dielectric properties of bismuth pyrochlores, Solid State Communications 100 (7) (1996) 529–534.

[11] B. Nguyen, Y. Liu, R.L. Withers, The local crystal chemistry and dielectric properties of the cubic pyrochlore phase in the Bi_2O_3-$M_2ONb_2O_5$ (M_2=Ni^{2+} and Mg^{2+}) systems, Journal of Solid State Chemistry 180 (2007) 49–557.

[12] L. Li, X. Zhang, L. Ji, P. Ning, Q. Liao, Dielectric properties and electrical behaviors of tunable $Bi_{1.5}MgNb_{1.5}O_7$ thin films, Ceramics International 38 (2012) 3541–3545.

[13] L. Gao, S. Jiang, Y. Li, Effects of growth conditions on structure and dielectric properties of bismuth-magnesium niobate thin films, Physics Procedia 32 (2012) 340–344.

[14] L. Gao, S. Jiang, R. Li, B. Li, Y. Li, Structure and dielectric properties of sputtered bismuth magnesium niobate thin films, Thin Solid Films 520 (2012) 6295–6298.

[15] S.S. Kim, W.J. Kim, Electrical properties of sol-gel derived pyrochlore-type bismuth magnesium niobate $Bi_2(Mg_{1/3}Nb_{2/3})_2O_7$ thin films, Journal of Crystal Growth 281 (2005) 432–439.

[16] J.H. Park, C.J. Xian, N.J. Seong, S.G. Yoon, S.H. Son, J.M. Chung, J.S. Moon, H.J. Jin, S.E. Lee, J.W. Lee, H.D. Kang, Y.K. Chung, Y.S. Oh, Realization of a high capacitance density in $Bi_2Mg_{2/3}Nb_{4/3}O_7$ pyrochlore thin films deposited directly on polymer substrates for embedded capacitor applications, Applied Physics Letters 89 (2006) 232910.

[17] C.J. Xian, J.H. Park, S.G. Yoon, J.S. Moon, S.T. Lim, S.H. Sohn, H.M. Jung, Y. Shin, W.C. Kim, M.K. Jeon, S.I. Woo, Effect of thickness on electrical properties of bismuth-magnesium niobate pyrochlore thin films deposited at low temperature, Journal of Applied Physics 101 (2007) 084114.

[18] P.Y. Tan, K.B. Tan, C.C. Khaw, Z. Zainal, S.K. Chen, M.P. Chon, Structural and electrical properties of bismuth magnesium tantalate pyrochlores, Ceramics International 38 (2012) 5401–5409.

[19] LMGP-Suite Suite of Programs for the interpretation of X-ray Experiment, by Jean Laugier and Bernard Bochu, ENSP/Laboratoire des Mat Matériaux et du Génie Physique, BP 46. 38042 Saint Martin d'Hères, France, http://www.inpg.fr/LMGP and http://www.ccp14.ac.uk/tutorial/lmgp/.

[20] G.C. Miles, A.R. West, Pyrochlore phases in the system ZnO-Bi_2O_3-Sb_2O_5: II. Crystal structures of $Zn_2Bi_{3.08}Sb_{2.92}O_{14+\delta}$ and $Zn_{2+x}Bi_{2.96-(x-y)}Sb_{3.04-y}O_{14.04+\delta}$, Solid State Sciences 8 (2006) 1422–1429.

[21] K.B. Tan, C.K. Lee, Z. Zainal, C.C. Khaw, Y.P. Tan, H. Shaari, Reaction study and phase formation in Bi_2O_3–ZnO–Nb_2O_5 ternary system, Pacific Journal of Science and Technology 9 (2008) 468–479.

[22] R.D. Shannon, Revised effective ionic radii and systematic studies of interatomic distances in halides and chalcogenides, Acta Crystallographica Section A: Fourndations of Crystallography 32 (1976) 751–767.

[23] K.B. Tan, C.C. Khaw, C.K. Lee, Z. Zainal, G.C. Miles, Structures and solid solution mechanisms of pyrochlore phases in the systems Bi_2O_3–ZnO–$(Nb,Ta)_2O_5$, Journal of Alloys and Compounds 508 (2010) 457–462.

[24] I. Levin, T.G. Amos, J.C. Nino, T.A. Vanderah, C.A. Randall, M.T. Lanagan, Structural study of an unusual cubic pyrochlore $Bi_{1.5}Zn_{0.92}Nb_{1.5}O_{6.92}$, Journal of Solid State Chemistry 168 (2002) 69–75.

[25] G.K. Williamson, W.H. Hall, X-ray line broadening from filed aluminium and wolfram, Acta Metallurgica 1 (1953) 22–31.

[26] M. Chen, D.B. Tanner, J.C. Nino, Infrared study of the phonon modes in bismuth pyrochlores, Physical Review B 72 (2005) 054303.

[27] J.T.S. Irvine, D.C. Sinclair, A.R. West, Electroceramics: characterization by impedance spectroscopy, Advanced Materials 2 (1990) 132–138.

[28] F.S. Morrison, D.C. Sinclair, A.R. West, Characterization of lanthanum-doped barium titanate ceramics using impedance spectroscopy, Journal of the American Ceramic Society 83 (2001) 531–538.

[29] C.C. Khaw, K.B. Tan, C.K. Lee, High temperature dielectric properties of cubic bismuth zinc tantalate, Ceramics International 35 (2009) 1473–1480.

[30] A.K. Jonscher, Dielectric relaxation in solids, Journal of Physics D: Applied Physics 32 (1999) R57–R70.

[31] S. Kamba, V. Porokhonskyy, A. Pashkin, V. Bovtun, J. Petzelt, Anomalous broad dielectric relaxation in $Bi_{1.5}Zn_{1.0}Nb_{1.5}O_7$ pyrochlore, Physical Review B 66 (2002) 054106.

[32] A.J. Bell, Calculation of dielectric properties from the superparaelectric model of relaxors, Journal of Physics: Condensed Matter 5 (1993) 8773–8792.

[33] R.D. Shannon, Dielectric polarizabilities of ions in oxides and fluorides, Journal of Applied Physics 73 (1993) 348–366.

[34] H. Du, X. Yao, Dielectric relaxation characteristics of bismuth zinc niobate pyrochlores containing titanium, Physica B 324 (2002) 121–126.

[35] H. Du, X. Yao, Structural trends and dielectric properties of Bi-based pyrochlores, Journal of Materials Science: Materials in Electronics 15 (2004) 613–616.

[36] S. Clima, G. Pourtois, A. Hardy, S.V. Elshocht, M.K.V. Bael, S.D. Gendt, D.J. Wouters, M. Heyns, J.A. Kittl, Dielectric response of Ta_2O_5, Nb_2O_5, and $NbTa_5$ from first-principles investigation, Journal of the Electrochemical Society 157 (2010) G20–G25.